Rock Mechanics and Rock Engineering (2019) 52:2815–2833
https://doi.org/10.1007/s00603-018-1720-x

ORIGINAL PAPER

Experimental Study of the Seepage Characteristics of Loaded Coal Under True Triaxial Conditions

Jiajia Liu[1,2,3,4] · Jianliang Gao[2,3,4] · Xuebo Zhang[2,3,4] · Gaini Jia[2] · Dan Wang[1,2]

Received: 11 May 2018 / Accepted: 17 December 2018 / Published online: 2 January 2019

Abstract

Gas-bearing, coal-bearing rocks are affected by geological structures and mechanical disturbances. A stress environment exists in an unequal three-way pressure state. To determine the mechanisms of stress change that influence the fissure evolution in stratified coal under true triaxial conditions, different stratifications (vertical, horizontal and oblique stratifications) are experimentally studied based on coal gas permeability. The coal samples are investigated using scanning electron microscopy and transmission electron microscopy to analyze the microstructure differences of the coal samples before and after loading. The results show that the permeability of the different stratified coal samples is exponentially related to the maximum principal stress, the intermediate principal stress, the minimum principal stress and the effective stress. The initial permeability of the vertically stratified coal samples is only 13.5%, which is 22.2% of that for skewed bedding. The bedding direction has a significant effect on the seepage characteristics of the coal samples. In the past, most scholars ignored the influence of bedding when conducting permeability tests. The results of this paper have important theoretical and practical value for optimizing the parameters of gas drainage, increasing the gas drainage rate and reducing the "greenhouse effect" caused by gas emissions.

Keywords True triaxial test · Layer structure · Gas seepage · Microstructure · Coal damage

List of Symbols

σ_1	Maximum principal stress
σ_2	Intermediate principal stress
σ_3	Minimum principal stress
D_m	Permeability loss of coal samples
k_0	Permeability of the initial coal sample during loading
k_m	Permeability of the coal sample at the end of the loading
k_b	Minimum permeability value of the coal sample during the entire loading process
ε_v^P	Volumetric strain increment
ε_{vi} $(i = 1, 2, 3 \ldots, n)$	Volumetric strain
ε_v	Volume strain
ε_1	Direction of the maximum principal stress
ε_2	Direction of the intermediate principal stress
ε_3	Direction of the minimum principal stress
τ	Shear stress
σ_m	Average normal stress
τ_ψ	Shear stress on the ψ plane
σ_ψ	Normal stress on the ψ plane

✉ Jiajia Liu
liujiajia@hpu.edu.cn

✉ Xuebo Zhang
aa19851985@sina.com

[1] State Key Laboratory Cultivation Base for Gas Geology and Gas Control, Henan Polytechnic University, Jiaozuo 454003, People's Republic of China

[2] School of Safety Science and Engineering, Henan Polytechnic University, 2001 Century Ave., High-Tech Campus, Jiaozuo 454000, Henan, People's Republic of China

[3] State and Local Joint Engineering Laboratory for Gas Drainage and Ground Control of Deep Mines, Henan Polytechnic University, Jiaozuo 454003, China

[4] The Collaborative Innovation Center of Coal Safety Production of Henan Province, Jiaozuo 454003, China

1 Introduction

Because the three-way stress associated with loaded coal is related to the occurrence of coal seams, the geological conditions of the coal seam dips, and mechanical disturbances, such as tectonic movements, the stress conditions are generally three-dimensional and of unequal pressures. Mining operations, such as gas drainage and coal mining, can also cause stress redistribution, which can lead to local stress concentrations. The stress environment is also in a three-dimensional unequal pressure state, or a true triaxial stress state (maximum principal stress σ_1 > intermediate principal stress σ_2 > minimum principal stress σ_3). However, a seepage test of loaded coal usually occurs in uniaxial ($\sigma_1 > \sigma_2 = \sigma_3 = 0$) or pseudotriaxial ($\sigma_1 > \sigma_2 = \sigma_3$) form. In such tests, the experimental environment is in a simple stress state, and the special case of coal-bearing bodies is often inconsistent with the actual conditions in the field. In most cases, gas migration in coal seams and the destruction and deformation of coal bodies occur under complex stress conditions. The uniaxial, pseudotriaxial and true triaxial coal stress distributions are shown in Fig. 1.

The inhomogeneity, pore fissures, stratification structure and coal body pressure observed during the coal formation process in China directly affect the deformation mechanics of coal, resulting in obvious differences in the directions of the coal fracture evolution, expansion and seepage. Previously, the seepage properties of rocks have been studied under true triaxial conditions. Liu et al. presented measurements of the permeability upon changing the principal stresses and flow directions of coal under different true triaxial stress conditions obtained using a newly developed multifunctional true triaxial geophysical (TTG) apparatus. However, the authors ignored the influences of vertical, parallel and skewed bedding when conducting permeability tests of coal samples (Liu et al. 2018).

Many scholars have carried out true triaxial experimental research on rock and determined the influence of the intermediate principal stress on rock permeability (Takahashi et al. 2013; Kaunda 2014; Ingraham et al. 2013). Samuelson et al. posited that the pore fluid pressure has an important effect on the frictional strength and stability of tectonic faults and reported laboratory measurements of the porosity changes associated with transient increases in the shear velocity during frictional sliding within a simulated fine-grained quartz fault gouge. The experiments were conducted in a novel true triaxial pressure vessel with a double-direct shear geometry (Samuelson et al. 2009). Kwasniewski et al. presented and discussed a general failure criterion to predict the ultimate strength of rocks under both axisymmetric and true triaxial (asymmetric) compressive stress conditions (Kwasniewski 2013). Tan et al. conducted a series of triaxial fracture experiments using natural outcrops to jointly exploit unconventional gas resources, such as coalbed methane (CBM), and the results of the novel method provided theoretical support for effective field implementation in coexploited strata (Tan et al. 2017). Some scholars have carried out true triaxial loading and unloading experiments on high-stress rock, loess, granite, sandstone, gravel clay and other materials and obtained anisotropic deformation characteristics. (Nasseri et al. 2014; Du et al. 2013; Deng and Shao 2013; Miao et al. 2011; Zhang et al. 2010; Xie and He 2010; Gao et al. 2017). Many scholars have carried out experimental research on gas-containing coal under the condition of true triaxial loading and unloading and obtained the seepage characteristics of the coal seam gas in an anisotropic environment (Massarotto et al. 2003; Nie et al. 2009; Gong et al. 2011; Xu 2003).

In the development of the true triaxial test system. some scholars have carried out mechanical tests on coal under different stress conditions through a self-developed true triaxial test system and obtained the gas migration and seepage characteristics of the coal seam (Yin et al. 2015; Li et al. 2016a, b, c; Xu et al. 2010; Feng et al. 2016; Faoro et al. 2009; Takahashi 2007). For the first time, Li used a layered combination of coal seams and rock formations for true triaxial testing. The experiment considers the influence of different

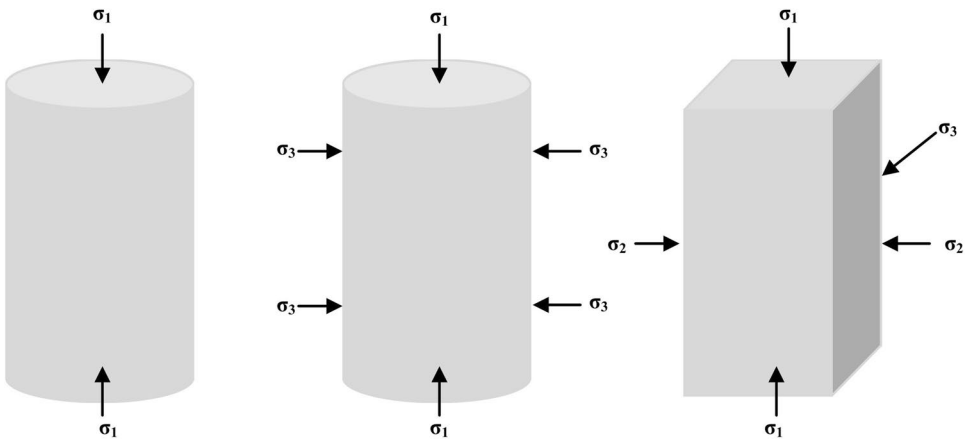

Fig. 1 Stress distribution in coal samples

geological and engineering factors on the propagation of natural cracks and obtains the permeability anisotropy of the coal, which makes the crack geometry more complex, and the experimental results provide new theoretical guidance for the development of coalbed methane (Li et al. 2014). Karev VI et al. used a complex triaxial independent loading test to study the fracture conditions of layered rocks composed of productive oil and gas strata (Karev VI et al. 2016). Lei simulated the effect of multiaxial (true triaxial) stress loading on the permeability of fractured rock. The simulation results show that pre-existing cracks show stronger flow characteristics, which is used to understand the nonuniform flow of underground fluids and improve large-scale water inrush. The evaluation of penetration is also important (Lei et al. 2017). Many scholars have established anisotropic permeability models for rocks under true triaxial stress conditions. Some scholars have established permeability models for gas-bearing coals and considered the effects of the Klinkenberg effect on the gas seepage characteristics (Li et al. 2016a, b, c; Wang and Zhang 2013; Wang et al. 2015).

Hadi Mosleh et al. presented an experimental study on the permeability evolution in a high-rank coal from a South Wales coalfield. Due to the interaction with different types of gases, the research results show a considerable reduction in the permeability at a CO_2 pressure above 1.5 MPa that is correlated with the coal matrix swelling induced by CO_2 adsorption. Niu et al. aimed to characterize the coal permeability by combining laboratory measurements with a simple gas slippage model that explains the rebound phenomenon. Shi et al. presented permeability ratios for both constant confining tests and constant effective stress tests that were primarily determined by matrix-fracture interactions, including sorption-induced swelling/shrinking, through transient effective stresses in matrixes and fractures, but these authors ignored the geological conditions of coal seam dips and mechanical disturbances, such as tectonic movements. Additionally, the stress conditions are generally three-dimensional and of unequal pressures, and these authors ignored the effects of bedding (vertical, parallel and Oblique) in the coal sample permeability test. (Hadi et al. 2018; Niu et al. 2018; Shi et al. 2018). Zhao used an acoustic emission monitoring system to carry out a true triaxial strain blasting test of granite and obtained the relationship between the acoustic emission and the stress and strain of the granite (Zhao and Cai 2015). Huang used a large-scale true triaxial hydraulic blasting experimental system and an acoustic emission three-dimensional positioning system for a hydraulic blasting experiment involving cement mortar test blocks to study the relevant characteristics of hydraulic blasting crack morphology (Huang and Li 2015).

Research is greatly needed on the influence of different bedding structures (vertical, parallel and skewed bedding) and the seepage characteristics of loaded coal under true axial conditions. Additionally, the effects of different loading processes on the deformation mechanisms and permeability evolution of cracks in coal bores remain unclear. Based on a true three-axis fluid–solid coupled seepage test platform combined with the mechanical characteristics of the coal mining process, the seepage characteristics of a coalbed were studied under different loading stress paths. Experiments were conducted to study the influence of different stress changes on the seepage trends of coal under a load.

2 Experimental Device and Methods

2.1 Preparation and Processing of Coal Samples

The coal samples used in the experiment were taken from the 29,031 working face of a mine, and the coal type was lean coal with a high degree of metamorphism. The coal seam has a strong layered structure. First, fresh large lumps of coal with an obvious layered structure were collected (the length, width, and height of each coal lump were greater than 20 cm), and the coal samples were then wrapped in plastic wrap and transported to the laboratory. Cutting machines were used to vertically and horizontally cut the samples. Each large piece of raw coal was processed into a cubic standard coal sample measuring $50 \times 50 \times 100$ mm, and the end surface of each coal sample was polished with a grinding machine to meet the requirements of the method for determining the physical and mechanical properties of coal and rock. The prepared coal samples were labeled and wrapped with plastic wrap. The bedding directions of the vertical bedding, parallel bedding and skewed bedding of the coal samples were 90°, 0°, and 60°, respectively. The specific sample production process is shown in Fig. 2.

According to the experimental requirements, to reduce the discreteness of the test data, three coal samples with no cracks, similar quality and uniform CT scan characteristics were selected for testing. A schematic diagram of the coal samples with different layering directions, including perpendicular to the stratified coal samples, parallel to the stratified coal samples and oblique to the stratified coal samples, is shown in Fig. 3.

2.2 Experimental Device Profile

The experimental equipment used in the true three-axis fluid–solid coupled seepage test included a servo hydraulic loading system, a pore pressure loading control system, a coal sample holder, a temperature control system, an experimental data acquisition system, and a vacuum degassing system. A physical image and schematic diagram of the experimental equipment are shown in Figs. 4 and 5, respectively.

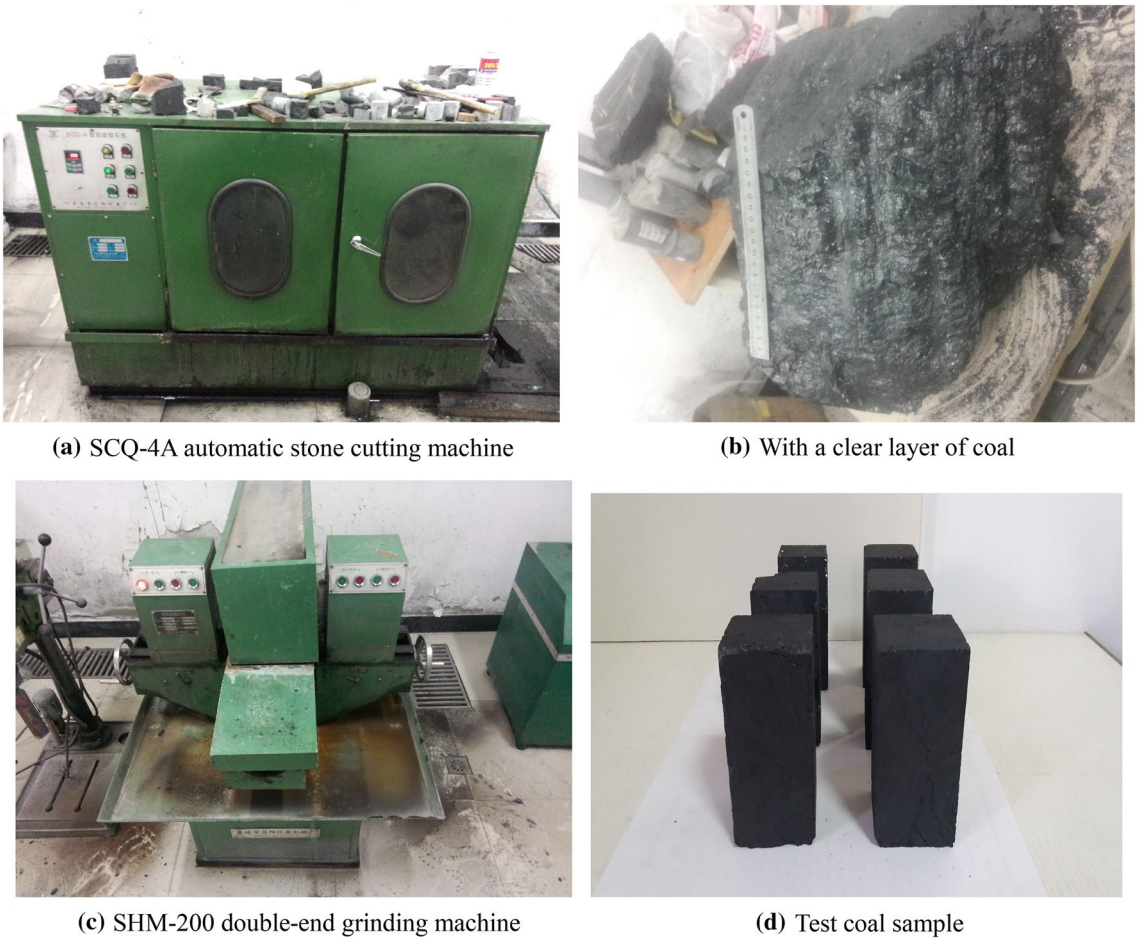

(a) SCQ-4A automatic stone cutting machine

(b) With a clear layer of coal

(c) SHM-200 double-end grinding machine

(d) Test coal sample

Fig. 2 Coal sample production process

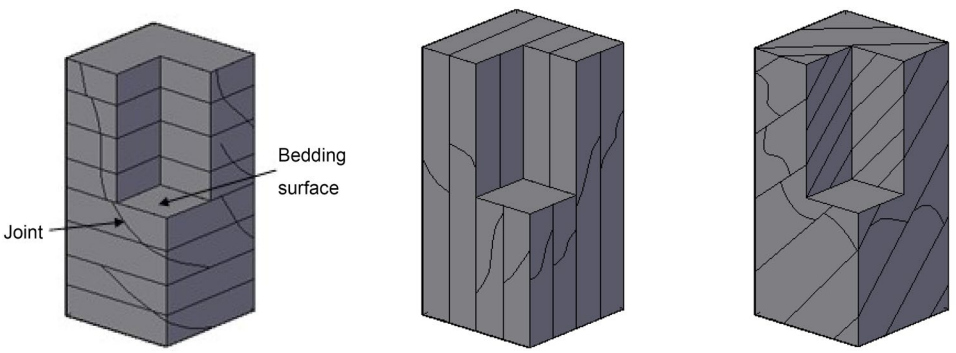

(a) Vertical beddings

(b) Parallel beddings

(c) Oblique beddings

Fig. 3 Schematic diagram of bedding fractures in different directions: **a** vertical bedding; **b** parallel bedding; and **c** oblique bedding

2.2.1 Servo Hydraulic Stress Loading System

The stress loading system adopts the servo hydraulic method for loading, and this method can achieve continuous stability and high loading precision. The system mainly consists of an HDH-250 servo loading device and a pressurizing tank. The servo device is loaded with distilled water. The specific stress loading process is as follows. First, the pipette of the servo loading device is placed into the distilled water cylinder. Then, the liquid suction valve of the servo loading device is opened, and the liquid absorption rate is set with the computer control interface to allow liquid suction at a given rate. The suction valve is closed to open the drain

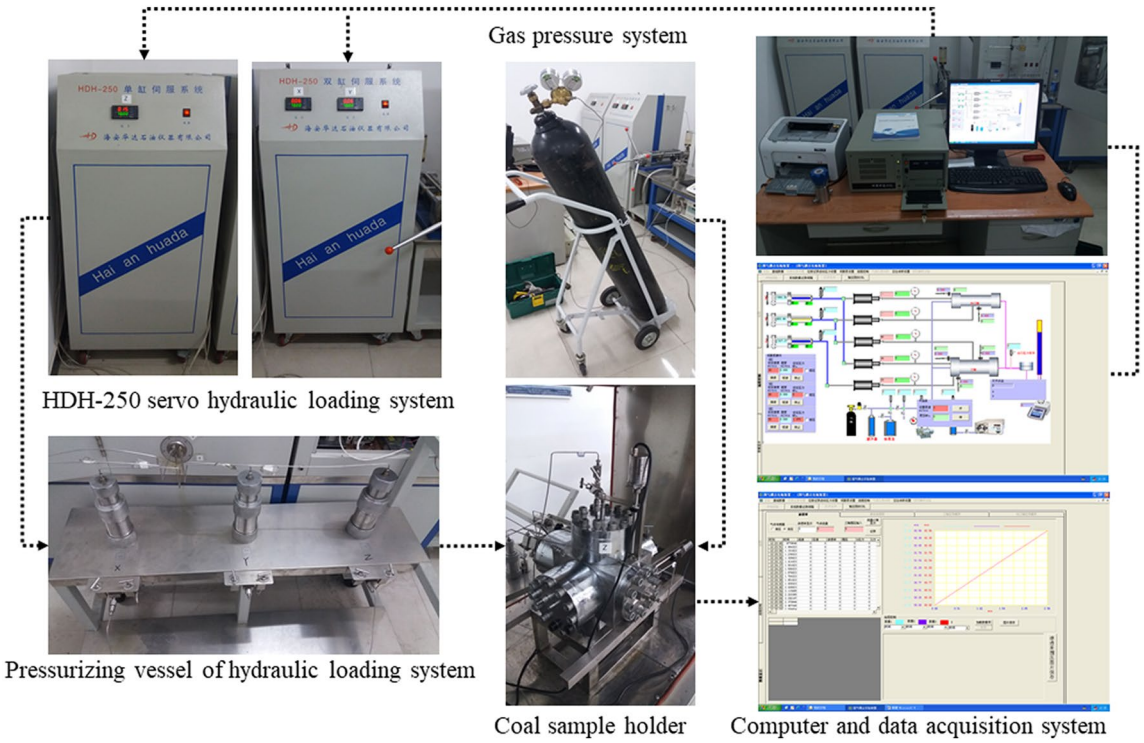

Fig. 4 Physical image of the experimental device

valve, and the booster tank is drained. Finally, the stress loading is completed using the booster tank.

2.2.2 Pore Pressure System and Coal Sample Holder

The gas pressure gauge system is composed of a gas pressure gauge, a gas bottle, a pressure-reducing valve and a special gas pipe. The test gas used is 99.99% nitrogen. The pressure of the gas at the gas inlet is regulated by the pressure-reducing valve. All gas lines are equipped with a high-pressure seal combination pad to ensure an airtight experiment.

The sample holders are composed of high-precision stainless steel with 12-thread snap fasteners at each end in the *X*, *Y*, and *Z* directions. Both the screw-on clips and the cartridge holder cover have spring washers, a sealing cap and a cavity in a heat-shrinkable tube equipped with a rubber ring to ensure the sealing of the coal sample holder. The gas pressure system and sample holder are shown in Fig. 4.

2.2.3 Temperature Control System

Experimental temperature control is achieved via a precision incubator that is electrically heated, and the temperature of the incubator is set to the experimental temperature before each experiment. The incubator temperature control error is ± 0.1 °C, the maximum temperature is 85 °C, and the specific incubator control switch is shown in Fig. 4 (the red button at the top of the device).

2.2.4 Vacuum Degassing System

The vacuum degassing system mainly consists of vacuum pumps, pipes and other components. The vacuum pump is model 2XZ-4, with a pumping rate of 4 L/s and speed of 1400 r/min. Before starting the experiment, the vacuum pump is opened to degas the experimental system and to ensure that the experimental system approximates an absolute vacuum. The vacuum system is then closed to maintain a negative pressure within 2 h and to complete the vacuum degassing process.

2.2.5 Data Acquisition System

The data acquisition system consists of a computer, an acquisition card, an exit flow test device and the related test software. The specific test data acquisition system is shown in Fig. 4. The outlet flow test device includes a measuring cylinder, a fixing rack, a rubber hose, and a stopwatch. The bubble method is used to perform the test, and the test software automatically inputs the gas flow rate and collects data on the time required for the bubbles to rise a fixed distance. The computer test software can also automatically acquire

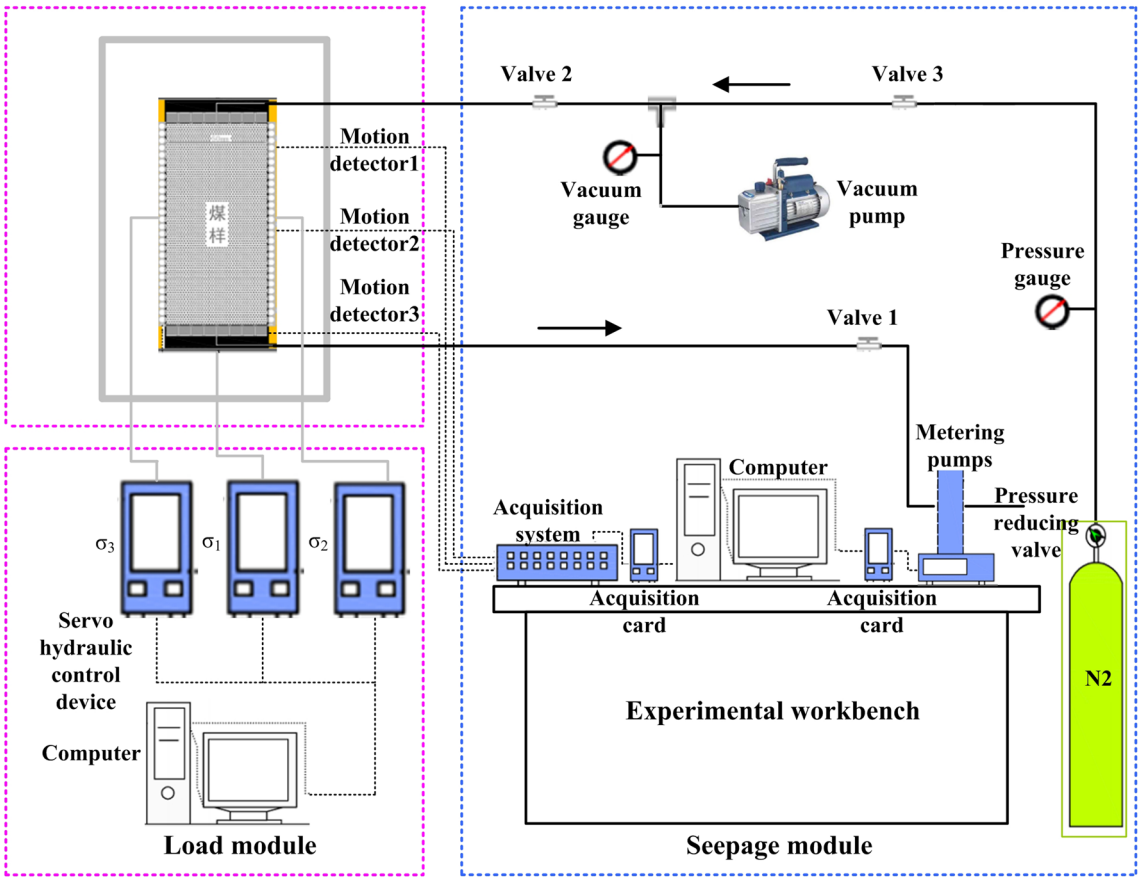

Fig. 5 Schematic diagram of the experimental device

the stress, temperature and other experimental data to ensure the continuity of the experimental data acquisition.

2.3 Experimental Program and Steps

Underground gas drainage, coal seam excavation, drilling and other mining activities can lead to stress redistribution and local stress concentrations, which seriously affect gas accumulation and seepage; therefore, understanding the load path in load-bearing coal is critical. However, considering the constraints of the experimental equipment and the experimental conditions, studies are typically conducted by simplifying the stress path of the experiment. In this experiment, the three-way stress of load-bearing coal is affected by the presence of coal seams, the geological conditions of the coal seam dips, and mechanical perturbations, such as tectonic movements. Additionally, the stress conditions are generally associated with a three-dimensional unequal pressure state. In this experiment, the maximum principal stress σ_1 in the X direction, the intermediate principal stress σ_2 in the Y direction, and the minimum principal stress σ_3 in the Z direction are used to study the seepage characteristics under different triaxial conditions. The specific experimental stress path is given below.

Stress path 1 The gas source is nitrogen, and the gas pressure is 1.0 MPa. Because the coal that has not been affected by the mining is in a hydrostatic pressure condition, the triaxial stress $\sigma_1=\sigma_2=\sigma_3=2$ MPa should be applied stepwise according to three isobaric pressures: Constants σ_2 and σ_3 remain unchanged, step loading σ_1 to 16 MPa at a rate of 0.1 MPa/step; constants σ_1 and σ_3 remain unchanged, and the σ_2 load is increased to 16 MPa at a rate of 0.1 MPa/step; constants σ_1 and σ_2 remain unchanged, and the σ_3 load is increased to 16 MPa at a rate of 0.1 MPa/step. In a seepage experiment, the pore pressure should be less than σ_2 and σ_3.

Stress path 2: The gas source is nitrogen, and the gas pressure is 1.0 MPa. First, a triaxial stress is gradually applied until the predetermined stress $\sigma_1=\sigma_2=\sigma_3=2$ MPa according to the three-way isobaric conditions. Constants σ_2 and σ_3 remain unchanged, and σ_1 loading is performed at a rate of 0.1 MPa/step until the coal samples are destroyed. Regardless of the loading and unloading values used in the seepage experiment, the experiment must have a pore pressure less than σ_2 and σ_3. The specific experimental scheme and different stress loading paths are shown in Table 1 and Fig. 6.

Table 1 Experimental program

Load	Time interval	Pressure/MPa	Maximum principal stress/MPa	Intermediate principal stress/MPa	Minimum principal stress/MPa	Effective stress/MPa	Remarks
Load 1	1	1.0	2	2	2	1.45	Loading at 0.1 MPa/step speed
	2	1.0	4	2	2	2.12	
	3	1.0	6	2	2	2.78	
	4	1.0	8	2	2	3.45	
	5	1.0	10	2	2	4.12	
	6	1.0	12	2	2	4.78	
	7	1.0	14	2	2	5.45	
	8	1.0	16	2	2	6.12	
Load 2	1	1.0	16	2	2	6.12	
	2	1.0	16	4	2	6.78	Loading at 0.1 MPa/step speed
	3	1.0	16	6	2	7.45	
	4	1.0	16	8	2	8.12	
	5	1.0	16	10	2	8.78	
	6	1.0	16	12	2	9.45	
	7	1.0	16	14	2	10.12	
	8	1.0	16	16	2	10.78	
Load 3	1	1.0	16	16	2	10.78	Loading at 0.1 MPa/step speed
	2	1.0	16	16	4	11.45	
	3	1.0	16	16	6	12.12	
	4	1.0	16	16	8	12.78	
	5	1.0	16	16	10	13.45	
	6	1.0	16	16	12	14.12	
	7	1.0	16	16	14	14.78	
	8	1.0	16	16	16	15.45	
Load 4	1	1.0	2	2	2	1.45	Loading at 0.1 MPa/step speed until coal sample damaged
	2	1.0	3	2	2	1.78	
	3	1.0	4	2	2	2.12	
	4	1.0	5	2	2	2.45	
	5	1.0	6	2	2	2.78	
	–	–	–	–	–	–	
	–	–	–	–	–	–	
	N	1.0	N	2	2	N	

The experimental steps are as follows.

1. *Check the seal* First, test the sealing ability of the piping system of the experimental device to avoid leakage during the experiment and to ensure that reliable results are obtained.
2. *Dry the coal samples* To eliminate the effect of moisture on the test results, the experimental coal samples are placed in a drying box with a thermostat temperature 333 K for 24 h and then weighed. The coal sample is dried until its weight does not change.
3. *Positioning the sample* First, apply a layer of 704 silica gel to the coal sample around the coal wall and then place each coal sample into a rubber sleeve. The coal sample and the gap should be as close as possible, and the gas should not flow through the gap between the coal sample and the rubber sleeve. Second, connect the data acquisition system and other systems, and the entire system is connected to the incubator. Finally, ensure that the experimental environmental temperature is constant at 303 K.
4. *Degassing* Verify that the experimental system is correctly connected and then check the integrity of the experimental system, including the tightness of the connections. Next, check that the experimental temperature and the environment reflect the preset temperature and use two vacuum pumps at the inlet and outlet of the coal sample and a degassing system to ensure that the vacuum conditions remain constant for 2 h after being closed to complete the vacuum degassing process.

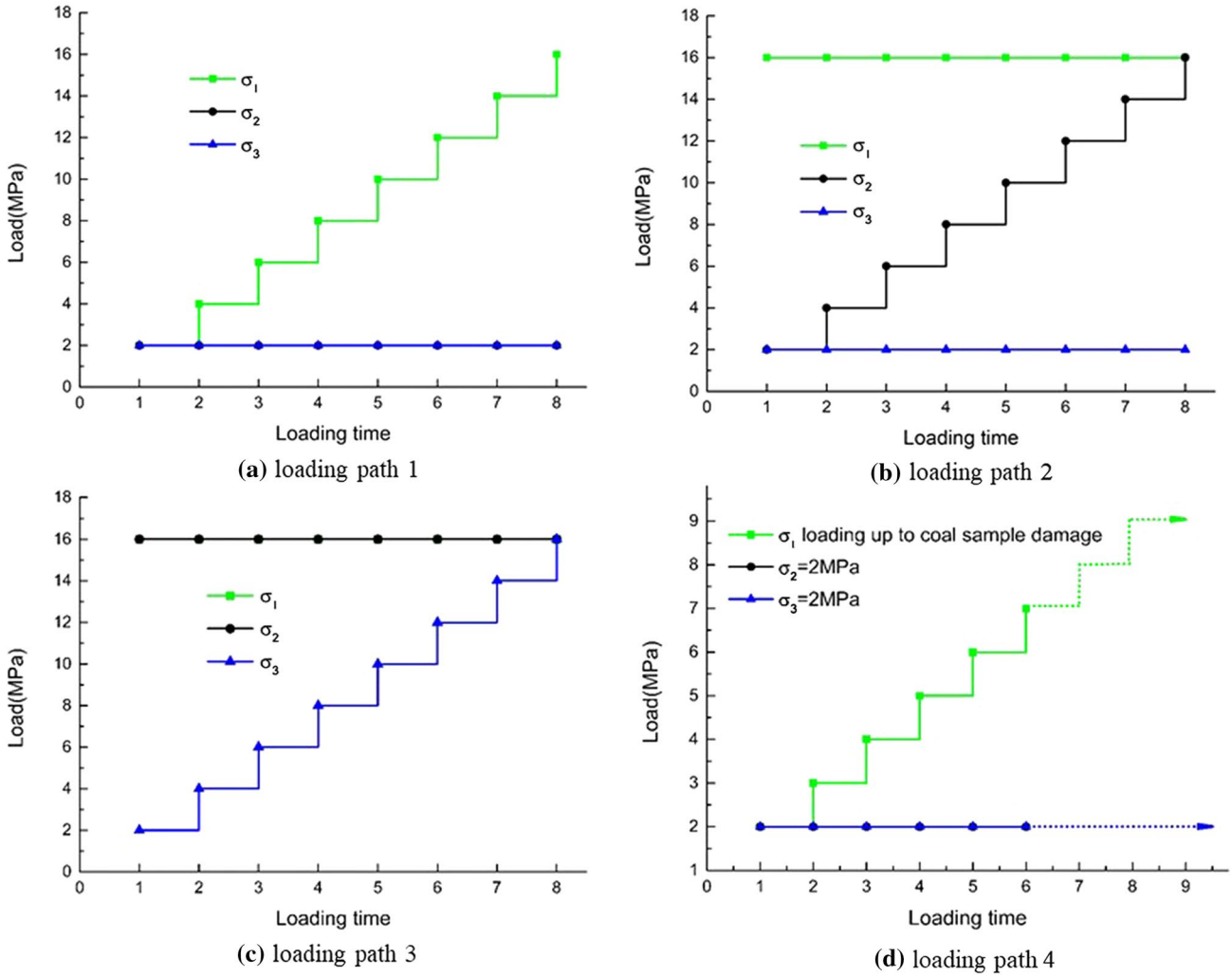

Fig. 6 Different stress loading paths: **a** loading path 1; **b** loading path 2; **c** loading path 3; and **d** loading path 4

5. *Gas adsorption balance* After the vacuum degassing of the experimental system is complete, the experimental pipeline system is filled with 99.99% nitrogen gas to a predetermined volume. To compensate for gas pressure variations over time, the gas pressure changes at the gas inlet and outlet should be noted. These changes are recorded with a pressure gauge. When the strain change rate is less than 2×10^{-4} h/1, it is considered that the coal sample has reached adsorption–desorption equilibrium.
6. *Permeability determination* After the gas adsorption equilibrium is reached, open the outlet valve of the experimental system, measure the outlet flow and record the data until the gas flow at the outlet is stable. Continuously measure the gas flow of the five groups. According to the stress path in the experimental scheme, gradually complete the experiment involving the coal seepage flow load.
7. *Sample replacement* Coal samples with vertical, parallel and skewed stratifications are used in three groups of nine experiments. When a group of experiments is complete, remove the coal sample holder after the destruction of the coal sample. Then, repeat steps (1)–(6) for the next set of load-bearing coal seepage experiments.

3 Experiments on the Seepage Characteristics of Loaded Coal

3.1 Percolation Characteristics of the Load in Vertically Stratified Coal Samples

3.1.1 Permeability Evolution of Vertically Stratified Coal Samples

According to the preselected experimental method and the set conditions of stress path #1, a vertical triaxial coal permeability test was conducted with the true triaxial

coal-bearing seepage experimental device. First, the three axial stresses were set so $\sigma_1=\sigma_2=\sigma_3=2$ MPa. Then, σ_2 and σ_3 remained unchanged, and σ_1 increased to 16 MPa at a rate of 0.1 MPa/step in the seepage test. The experimental results are shown in Fig. 7a. This procedure was followed by keeping σ_1 and σ_3 constant while increasing σ_2 to 16 MPa at a rate of 0.1 MPa/step. The associated experimental results are shown in Fig. 7b. Finally, σ_1 and σ_2 were held constant, and σ_3 was increased to 16 MPa at a rate of 0.1 MPa/step. These experimental results are shown in Fig. 7c.

An analysis of Fig. 7 indicates that the initial permeability of the vertically stratified coal samples is 0.0181 mD, but it decreases to 0.00384 mD by the end of the loading, a decrease of 78.9%. At the maximum principal stress σ_1 at the end of the loading stage, the permeability decreases to 0.00756 mD and then increases to 0.01066 mD. At the end of the intermediate principal stress σ_2 loading stage, Permeability decreased to 0.00243 mD, reduced by 0.005%, and finally reduced to 0.00384 mD; thus, the permeability decreases overall by 0.00129 mD. According to Fig. 7, the maximum principal stress σ_1, the intermediate principal stress σ_2, the minimum principal stress σ_3 and the permeability curves are plotted to obtain the fitting equation among the parameters as follows.

$$\begin{cases} k = 0.0058 + 0.0165\exp\left[-0.1434\left(\sigma_1\right)\right]\left(R^2 = 0.9866,\ \sigma_2 = 2\ \text{MPa},\ \sigma_3 = 2\ \text{MPa}\right) \\ k = 0.0051 + 0.0041\exp\left[-0.2661\left(\sigma_2\right)\right]\left(R^2 = 0.9917,\ \sigma_1 = 16\ \text{MPa},\ \sigma_3 = 2\ \text{MPa}\right) \\ k = 0.0038 + 0.0021\exp\left[-0.2173\left(\sigma_3\right)\right]\left(R^2 = 0.9902,\ \sigma_1 = 16\ \text{MPa},\ \sigma_2 = 16\ \text{MPa}\right) \end{cases} \tag{1}$$

Equation (1) shows that under the experimental conditions of stress path #1, the permeability of the vertically stratified coal samples is exponentially related to the maximum principal stress, intermediate principal stress and minimum principal stress and that the permeability increases as the stress increases. The rate of decrease gradually diminishes and the fractures in the coal sample are more easily compressed and closed at the initial stage of maximum principal stress loading. The maximum permeability reduction at this stage was 74.1%, mainly because the loading direction was perpendicular to the maximum principal stress. Additionally, stress loading in this stage makes the pore fissures in the coal samples to compressing rapidly. The permeability decrease in the coal samples in the intermediate main stress loading stage is 16.9%, while that in the minimum main stress loading stage is only 9.0%. The specific permeability reduction is calculated as shown in Eq. 2.

According to the research results of Wang et al. (2012), a decrease in coal sample permeability can be evaluated according to the rate of the coal-based permeability loss. A greater rate of permeability damage reflects a greater reduction in the permeability of coal samples. In different stress loading stages, the permeability loss of coal samples D_m can be calculated as follows:

$$D_m = \frac{k_0 - k_m}{k_b} \times 100\% \tag{2}$$

where k_0 is the permeability of the initial coal sample during loading, k_m is the permeability of the coal sample at the end of the loading, and k_b is the minimum permeability value of the coal sample during the entire loading process.

$$\begin{cases} D_{m1} = \dfrac{k_0 - k_{m1}}{k_b} \times 100\% = 74.1\% \\ D_{m2} = \dfrac{k_0 - k_{m2}}{k_b} \times 100\% = 16.9\% \\ D_{m3} = \dfrac{k_0 - k_{m3}}{k_b} \times 100\% = 9.0\% \end{cases} \tag{3}$$

To further analyze the relationship between the effective stress and permeability during the entire loading phase, according to the experimentally derived permeability results, the variations in the permeability during the entire loading process are fit as shown in Fig. 8.

An analysis of Fig. 8 indicates that as the effective stress increases, the permeability gradually decreases, and the decrease in the initial permeability of the coal sample is relatively large. The permeability linearly decreases when loaded to 8 MPa. When the loading exceeds 8 MPa, further decreases in permeability are more gradual. Specifically, the increase in the effective stress causes the pore fissures to gradually compress and close, and the gas flow channels gradually shrink. The resistance to gas flowing through the coal seepage channel gradually increases. Therefore, an increase in the effective stress leads to a decrease in the permeability of the coal sample, and the permeability gradually stabilizes after a certain value is reached. Through a fitting analysis of the variations in the permeability of the vertical coal strata during loading, the fitting equation between the permeability and the effective stress can be obtained as follows.

$$k = 0.0039 + 0.0219\exp\left[-0.3152\left(\sigma_e\right)\right]\left(R^2 = 0.9923\right) \tag{4}$$

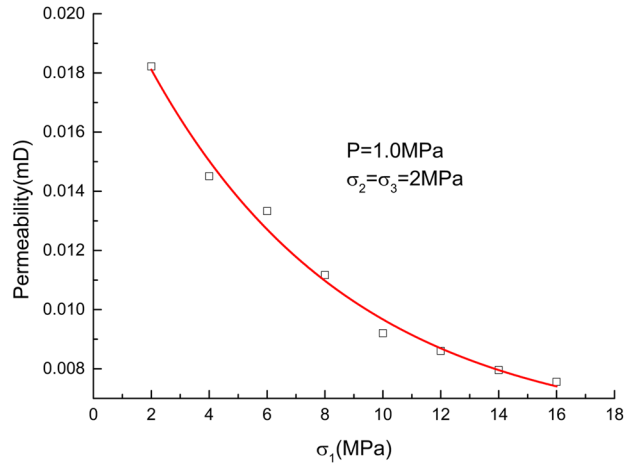

(a) Maximum principal pressure loading process

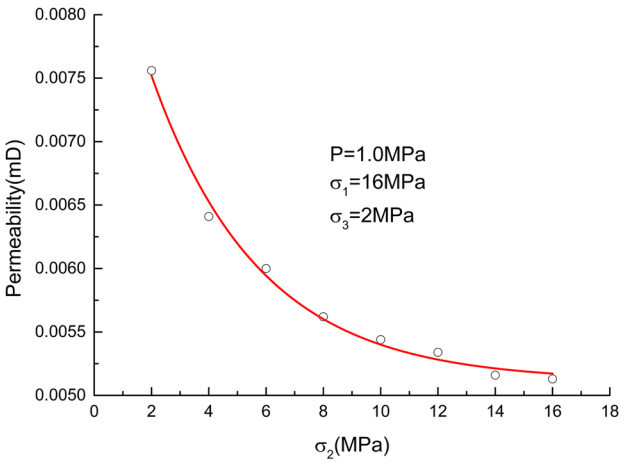

(b) Intermediate principal stress loading process

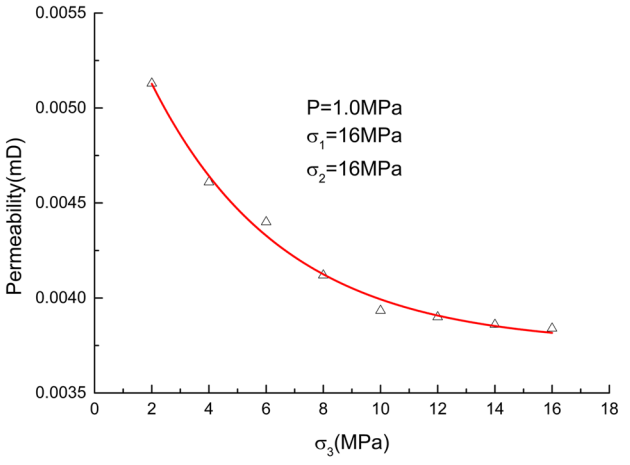

(c) Minimal principal pressure loading process

Fig. 7 Permeability evolution of the different principal pressure loading processes for the coal samples with vertical bedding

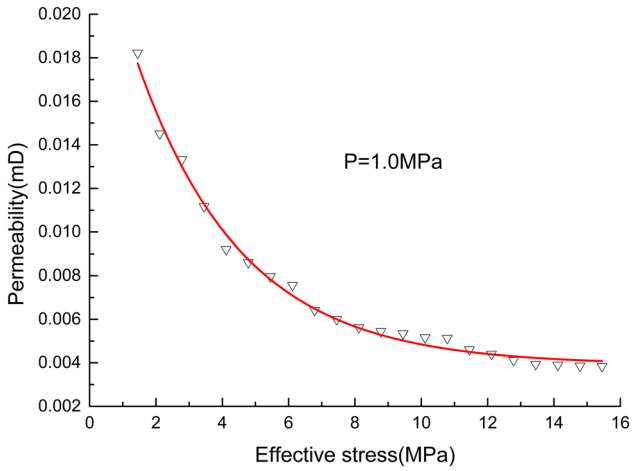

Fig. 8 Relationship between the effective stress and permeability of the vertically bedded coal samples

3.1.2 Compression–Expansion Boundary and Permeability Changes in the Coal Samples

With different layers of the coal samples involved in the deformation process, the stress state gradually transitions from compression deformation to expansion deformation, and the compression and expansion of the transition boundary create a compression-expansion boundary (compression–dilatancy boundary), referred to as the C–D boundary.

In the expansion area, in addition to the plastic deformation, the permeability increases with the expansion of the crack. Define the volumetric strain increment as $\varepsilon_{\mathrm{v}}^{\mathrm{P}}$:

$$\varepsilon_{\mathrm{v}}^{\mathrm{P}} = \varepsilon_{\mathrm{v}i+1} - \varepsilon_{\mathrm{v}i} \tag{5}$$

In the formula, $\varepsilon_{\mathrm{v}i}(i = 1, 2, 3 \ldots, n)$ is the volumetric strain, where the volume strain is ε_v:

$$\varepsilon_v = \varepsilon_1 + \varepsilon_2 + \varepsilon_3 \tag{6}$$

In the formula, ε_1 is the direction of the maximum principal stress, ε_2 is the direction of the intermediate principal stress, and ε_3 is the direction of the minimum principal stress. The compression is set to be positive, and the expansion is negative.

The C–D boundary conditions are as follows:

$$\begin{cases} \varepsilon_{\mathrm{v}}^{\mathrm{P}} > 0 \text{ (Compression)} \\ \varepsilon_{\mathrm{v}}^{\mathrm{P}} = 0 \text{ (C-D boundary)} \\ \varepsilon_{\mathrm{v}}^{\mathrm{P}} < 0 \text{ (Dilatancy)} \end{cases} \tag{7}$$

When $\varepsilon_{\mathrm{v}}^{\mathrm{P}} > 0$, the deformation of the coal body is mainly elastic compaction deformation, and some microcracks develop when the expansion is near, the porosity decreases, and the permeability decreases.

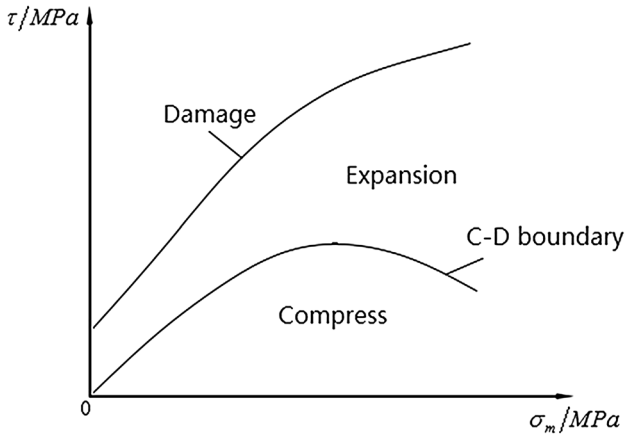

Fig. 9 C–D boundary diagram

When $\varepsilon_v^P < 0$ and the absolute value of the volumetric strain increment $\left|\varepsilon_v^P\right|$ is small, microcracks develop faster, but there is no connectivity between the cracks, and the permeability increases relatively slowly.

The specific boundary distribution is shown in Fig. 9.

In Fig. 9, τ is the shear stress, σ_m is the average normal stress, and the expression of the C–D boundary is as follows (Cristescu et al. 1994).

$$\begin{cases} X(\sigma_m,\tau) = -\tau + f_1\sigma_m^2 + f_2\sigma_m \\ \tau = \dfrac{\left[(\sigma_1-\sigma_2)^2 + (\sigma_1-\sigma_3)^2 + (\sigma_2-\sigma_3)^2\right]^{1/2}}{3} \\ \sigma_m = \dfrac{\sigma_1+\sigma_2+\sigma_3}{3} \end{cases} \tag{8}$$

The expression of using the principal stress is:

$$X(\sigma_1,\sigma_2,\sigma_3) = -\frac{\left[(\sigma_1-\sigma_2)^2 + (\sigma_1-\sigma_3)^2 + (\sigma_2-\sigma_3)^2\right]^{1/2}}{3} + f_1\left[\frac{(\sigma_1+\sigma_2+\sigma_3)}{3}\right]^2 + \frac{f_2(\sigma_1+\sigma_2+\sigma_3)}{3} \tag{9}$$

Additionally, the invariant expression can be given as follows.

$$\begin{cases} X(U_1,V_2) = -\sqrt{\dfrac{2}{3}}\sqrt{V_2} + f_1\dfrac{{U_1}^2}{9} + f_2\dfrac{U_1}{3} \\ U_1 = \sigma_1+\sigma_2+\sigma_3 \\ V_2 = \dfrac{\left[(\sigma_1-\sigma_2)^2 + (\sigma_1-\sigma_3)^2 + (\sigma_2-\sigma_3)^2\right]}{6} \end{cases} \tag{10}$$

According to $\tau_\psi = \sqrt{2V_2}, \sigma_\psi = U_1 \Big/ \sqrt{3}$, from a planar perspective, the shear stress and normal stress in the ψ plane can be expressed as follows.

$$X(\sigma_\psi,\tau_\psi) = -\frac{1}{\sqrt{3}}\tau_\psi + f_1\frac{\sigma_\psi^2}{3} + f_2\frac{\sigma_\psi}{\sqrt{3}} \tag{11}$$

Then, the relationship between the shear stress and normal stress in the meridian plane takes the following form.

$$\tau_\psi = f_1\frac{\sqrt{3}\sigma_\psi^2}{3} + f_2\sigma_\psi \tag{12}$$

The stress space shape of the C–D boundary is shown in Fig. 10.

The expansion boundary $\tau_\psi = f_1\frac{\sqrt{3}\sigma_\psi^2}{3} + f_2\sigma_\psi$ is a spatial surface with the parent line as the axis of rotation, and the ψ trace of the surface on the plane is a rounded hexagon. The C–D boundary is a boundary band rather than a boundary line.

The trajectory of the surface in the plane is a crisscrossing hexagon. The boundary of the expansion is based on the isosine line as the rotation axis.

According to the preselected experimental methods and the set conditions of stress path #2, a vertically stratified coal-based permeability test was conducted using a true three-axis fluid–structure interaction servo experimental device. First, the three-axis stress $\sigma_1=\sigma_2=\sigma_3=2$ MPa. Then, σ_2 and σ_3 remained unchanged, and σ_1 increased at a rate of 0.1 MPa/step until the coal sample was destroyed. When a coal sample began to change as the damage permeability increased, the stress loading was immediately stopped. At

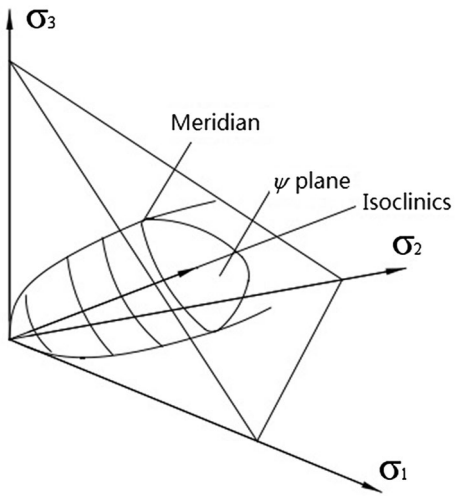

Fig. 10 Stress space form of the C–D boundary

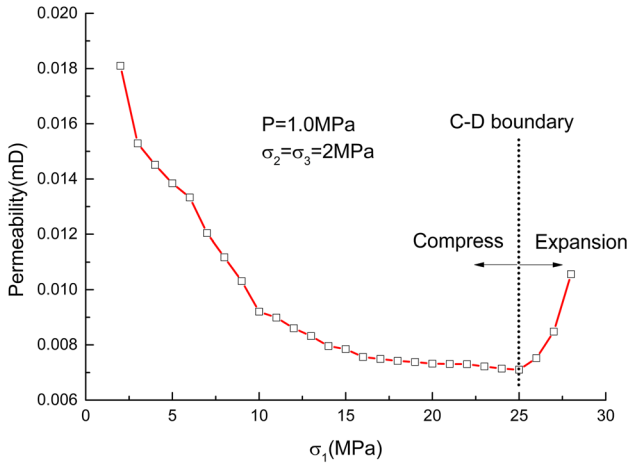

Fig. 11 Effect of the maximum principal stress loading process on the C–D boundary and permeability change in the vertically bedded coal samples

this point, integer values were used in the seepage test. The experimental results are shown in Fig. 11.

The constant intermediate principal stress is σ_2, and the minimum principal stress is σ_3 (i.e., $\sigma_2 = \sigma_3 = 2$ MPa). The maximum principal stress σ_1 is loaded until the coal sample is destroyed, and the permeability change during the deformation and destruction of the coal sample is roughly divided into three stages. In the first stage, cracks gradually develop, with a transition from compression to expansion in the coal samples. In the second stage, the permeability begins to slowly increase, and in the third stage, a large number of macrocracks appear, and the permeability rapidly increases. In this experiment, loading stops when the maximum principal stress σ_1 is reached to avoid destroying the rubber sleeve in the sample holder and damaging the experimental equipment. An analysis of Fig. 11 indicates that the permeability sharply decreases before the maximum principal stress σ_1 is loaded at 10 MPa, and the rate of the permeability reduction decreases when the load exceeds 10 MPa. When the maximum principal stress σ_1 is loaded to 25 MPa, the permeability begins to increase; that is, the maximum principal stress corresponding to the C–D boundary of the vertical coalbed is approximately 25 MPa.

3.2 Percolation Characteristics of the Load in Parallel Stratified Coal Samples

3.2.1 The Permeability Evolution of Parallel Layered Coal Samples

A permeability test was conducted with the true three-axis fluid–solid coupled servo experimental device. First, the triaxial stress $\sigma_1 = \sigma_2 = \sigma_3 = 2$ MPa was applied according to the three-way isobaric state, and σ_2 and σ_3 remained unchanged. The results of the experiment are shown in Fig. 12a. Second, σ_1 and σ_3 remained unchanged, and the loading was performed at a speed of 0.1 MPa/step. The loading σ_2 reached 16 MPa, and the experimental results are shown in Fig. 12b. Finally, σ_1 and σ_2 were held constant, and σ_3 was increased to 16 MPa at a rate of 0.1 MPa/step. These experimental results are shown in Fig. 12c.

An analysis of Fig. 12 indicates that the initial permeability of the parallel stratified coal samples is 0.1352 mD, and the permeability of the vertically stratified coal samples is only 13.5% of that of the parallel stratified strata. In the late stage of loading of the stratified coal, the permeability decreases by 0.00635 mD, or 95.3%. The permeability of the parallel stratified coal samples decreases much more than that of the vertically stratified coal samples, and the coal samples almost entirely lose their seepage capacity. For the maximum principal stress σ_1, the permeability of the coal sample decreases to 0.0594 mD, and the permeability decreases by 0.0758 mD by the end of the stage. For the intermediate principal stress σ_2, the permeability of the coal sample is 0.02358 mD, and the permeability decreases to 0.03582 mD at the end of the associated loading stage. The minimum principal stress σ_3 occurred at the end of the loading stage. The sample permeability was 0.00635 mD, and the permeability decreased by 0.01723 mD.

According to the maximum principal stress σ_1, the intermediate principal stress σ_2 and the minimum principal stress σ_3 shown in Fig. 12, the fitting equation relating these stresses and the permeability can be obtained as follows.

$$\begin{cases} k = 0.0582 + 0.1279\exp\left[-0.2551(\sigma_1)\right] \left(R^2 = 0.9941,\ \sigma_2 = 2\ \text{MPa},\ \sigma_3 = 2\ \text{MPa}\right) \\ k = 0.0167 + 0.0568\exp\left[-0.1419(\sigma_2)\right] \left(R^2 = 0.9946,\ \sigma_1 = 16\ \text{MPa},\ \sigma_3 = 2\ \text{MPa}\right) \\ k = 0.0056 + 0.0307\exp\left[-0.2582(\sigma_3)\right] \left(R^2 = 0.9899,\ \sigma_1 = 16\ \text{MPa},\ \sigma_2 = 16\ \text{MPa}\right) \end{cases} \quad (13)$$

Equation (13) shows that under the experimental conditions of stress path #1, the permeability of the parallel layered coal samples is exponentially related to the maximum principal stress, intermediate principal stress, and minimum principal stress. Stress loading decreases the permeability of the coal samples, and the fractures in the parallel stratified coal samples are gradually compressed and close during

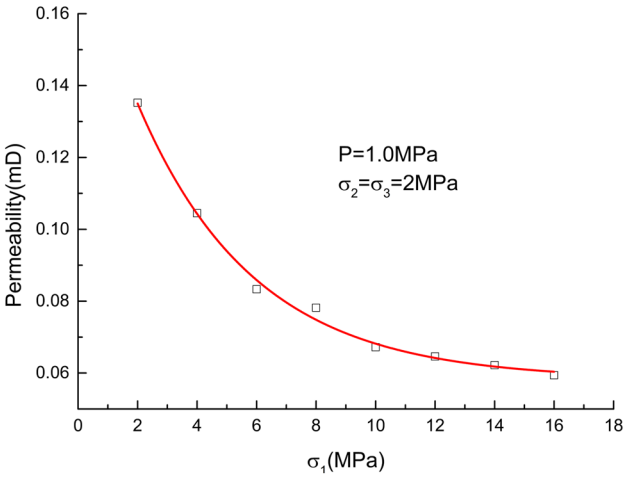

(a) Maximum principal pressure loading process

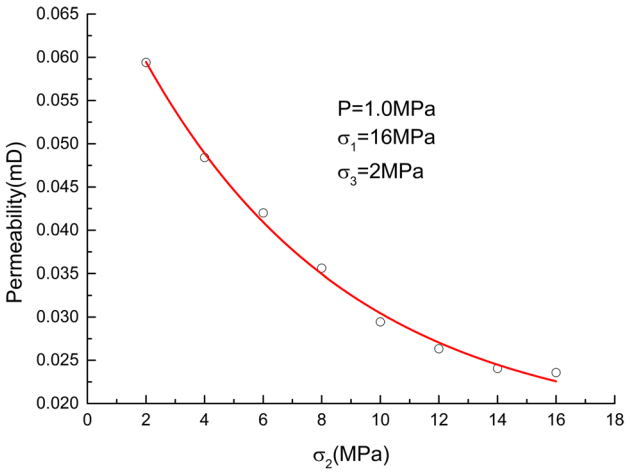

(b) Intermediate principal stress loading process

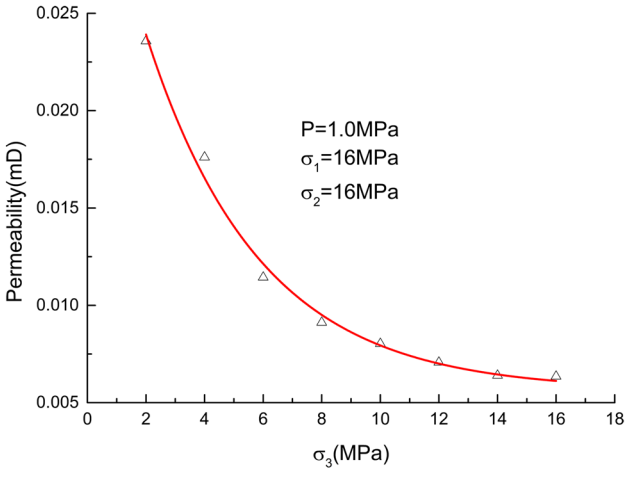

(c) Minimal principal pressure loading process

Fig. 12 Permeability evolution of the different principal pressure loading processes for the coal samples with parallel bedding

the initial stage of maximum principal stress loading. However, the permeability decrease is only 58.8% in this stage, which is lower than that (74.1%) associated with vertical stratification. The main reason for this difference is that the loading direction of the maximum principal stress is parallel to the direction of the bedding fracture surface of the coal sample. The loading in this stage does not completely close the bedding fracture surface. The permeability in the intermediate principal stress loading stage is 27.8%, which is higher than the decrease of 16.9% observed in the direction of vertical bedding. This difference is due to the loading of the intermediate principal stress, which further compresses the layered fracture surface. In the minimum primary stress loading stage, the permeability decreases only minimally, by 13.4%, and the specific permeability reduction can be calculated as follows.

According to Eq. (14), the maximum principal stress σ_1, the intermediate principal stress σ_2 and the minimum principal stress σ_3 are different. During the loading stage, the permeabilities of the coal samples are as follows.

$$\begin{cases} D_{\mathrm{m1}} = \dfrac{k_0 - k_{\mathrm{m1}}}{k_{\mathrm{b}}} \times 100\% = 58.8\% \\ D_{\mathrm{m2}} = \dfrac{k_0 - k_{\mathrm{m2}}}{k_{\mathrm{b}}} \times 100\% = 27.8\% \\ D_{\mathrm{m3}} = \dfrac{k_0 - k_{\mathrm{m3}}}{k_{\mathrm{b}}} \times 100\% = 13.4\% \end{cases} \tag{14}$$

According to the experimental results regarding the permeability of parallel layered coal samples, the relationship between the effective stress and permeability during the entire loading phase is analyzed, and the variation in permeability during the entire loading process is fitted as shown in Fig. 13.

An analysis of Fig. 13 indicates that the permeability decreases gradually as the effective stress increases during the loading process and that the initial permeability of the parallel stratified coal sample considerably decreases. These results are in agreement with the permeability trends of the vertically stratified coal samples. The permeability notably decreases before loading to 10 MPa and then decreases linearly. The decrease in permeability gradually decreases when the load exceeds 10 MPa. An increase in the effective stress leads to a decrease in the number of gas flow paths in the parallel stratified coal samples, and the resistance of the seepage flow paths in the coal body increases; i.e., an increase in the effective stress leads to a decrease in the coal sample permeability. Through fitting and analyzing the permeability trends during the process of parallel stratified coal sample loading, the fitting equation between the permeability and effective stress can be obtained as follows.

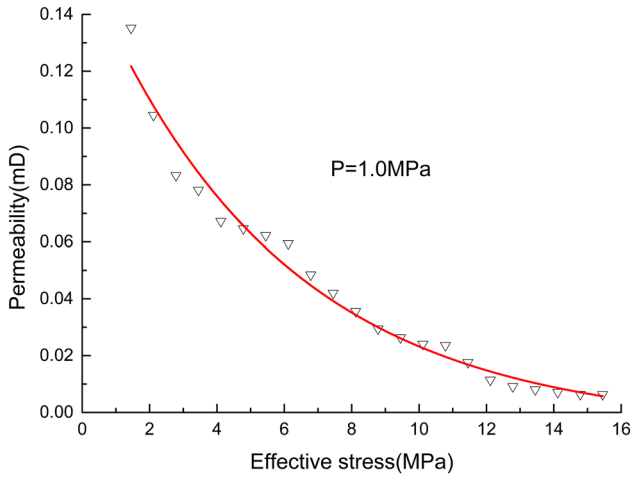

Fig. 13 Relationship between the effective stress and permeability in the coal loading process for the coal samples with parallel bedding

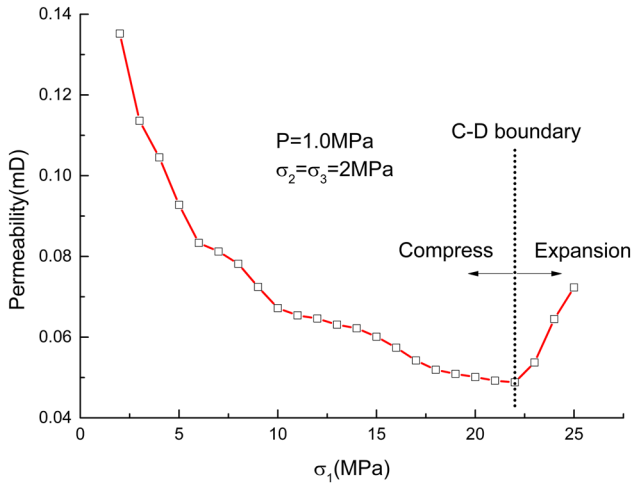

Fig. 14 Effect of the maximum principal stress loading failure process on the C–D boundary and permeability change in the coal samples with parallel bedding

$$k = -0.0053 + 0.1637\exp\left[-0.1748\left(\sigma_e\right)\right]\left(R^2 = 0.9752\right) \tag{15}$$

3.2.2 Compaction–Expansion Boundary and Permeability Changes in the Coal Samples

According to the preselected experimental methods and the set conditions of stress path #2, the experimental device for parallel three-axis fluid–solid coupled seepage flow is used to conduct a parallel permeability test of the coalbed permeability. First, according to the gradual application of three-way isostatic pressure, the stresses $\sigma_1 = \sigma_2 = \sigma_3 = 2$ MPa, σ_2 and σ_3 are held constant, and a step load of σ_1 is applied at a rate of 0.1 MPa/step until the coal

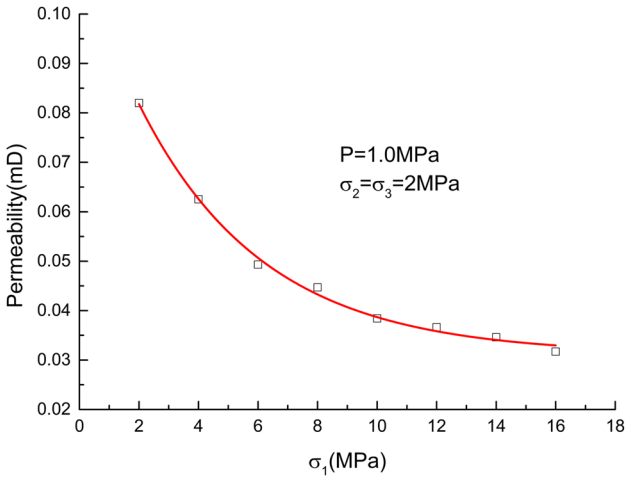

(a) Maximum principal pressure loading process

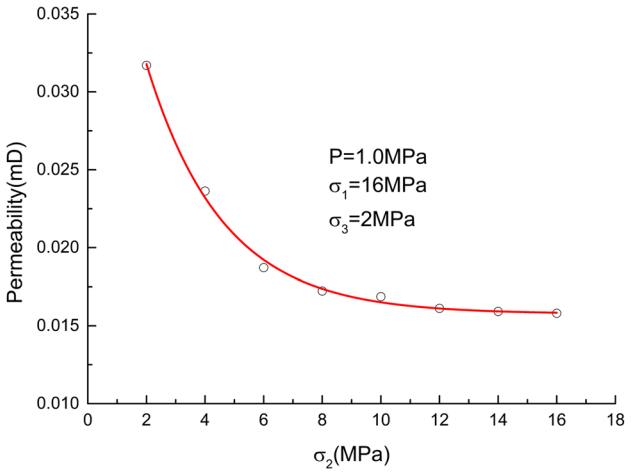

(b) Intermediate principal stress loading process

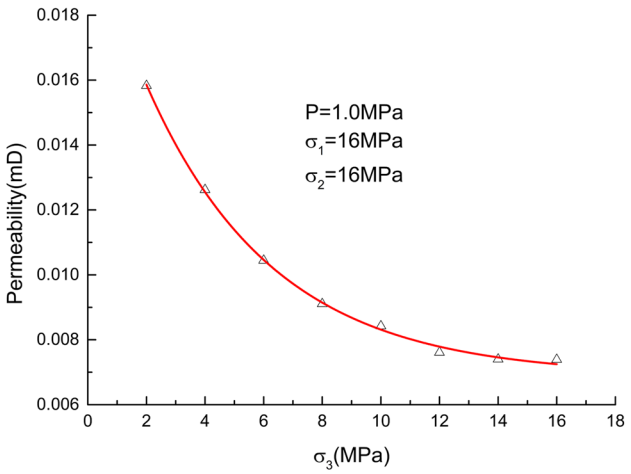

(c) Minimal principal pressure loading process

Fig. 15 Permeability evolution of the different principal pressure loading processes for the coal samples with skewed bedding

sample is destroyed. Thus, a load with an integer value is achieved in the seepage test. The experimental results are shown in Fig. 14.

The constant intermediate principal stress σ_2 and the minimum principal stress σ_3 are both 2 MPa. The maximum principal stress σ_1 is loaded until the coal sample is destroyed. The loading of the maximum principal stress σ_1 is immediately stopped before the coal sample is destroyed. 0.0158 mD, a decrease of 0.0159 mD. The permeability of the late stage loading of σ_3 is 0.00739 mD, a decrease of 0.0084 mD. The relations among the maximum principal stress σ_1, the intermediate principal stress σ_2, the minimum principal stress σ_3 and the permeability are obtained from the curves of these parameters according to Fig. 15. The equations are as follows.

$$\begin{cases} k = 0.0311 + 0.0815\exp\left[-0.2383(\sigma_1)\right] \left(R^2 = 0.9955,\ \sigma_2 = 2\ MPa,\ \sigma_3 = 2\ \text{MPa}\right) \\ k = 0.0157 + 0.0345\exp\left[-0.3835(\sigma_2)\right] \left(R^2 = 0.9962,\ \sigma_1 = 16\ \text{MPa},\ \sigma_3 = 2\ \text{MPa}\right) \\ k = 0.0069 + 0.1421\exp\left[-0.2302(\sigma_3)\right] \left(R^2 = 0.9983,\ \sigma_1 = 16\ \text{MPa},\ \sigma_2 = 16\ \text{MPa}\right) \end{cases} \tag{16}$$

An analysis of Fig. 14 indicates that the permeability of the parallel stratified coal samples decreases sharply at the initial loading of the maximum principal stress σ_1 and then decreases slowly, which is consistent with the trend of the vertical coal strata. When the load of σ_1 (the maximum principal stress) is 22 MPa, the permeability of the coal sample starts to increase; that is, the maximum principal stress corresponding to the C–D boundary of the parallel stratified coal samples is approximately 22 MPa, which is 3 MPa less than that of the vertically stratified coal samples.

3.3 Percolation Characteristics of the Load in Skewed Bedding Stratified Coal Samples

3.3.1 The Permeability Evolution Characteristics of Skewed Layered Coal Samples

According to the set experimental conditions, a permeability test of coal with skewed bedding was conducted using the fluid–solid coupled seepage device for a true triaxial coal-bearing fluid. The triaxial stresses $\sigma_1 = \sigma_2 = \sigma_3 = 2$ MPa, σ_2 and σ_3 remained unchanged, and σ_1 was loaded to 16 MPa at a rate of 0.1 MPa/step. A seepage test was conducted at every integer-value load. The experimental results are shown in Fig. 15a. Then, σ_1 and σ_3 were held constant, and σ_2 was increased to 16 MPa at a rate of 0.1 MPa/step. The associated experimental results are shown in Fig. 15b. Finally, σ_1 and σ_2 remained unchanged, and σ_3 was increased to 16 MPa at a rate of 0.1 MPa/step. These experimental results are shown in Fig. 15c.

Figure 15 shows the initial permeability of the coal samples with skewed stratification is 0.0822 mD, which is 0.6 times that of the parallel stratified coal samples, and the permeability of the coal samples decreases to 0.00739 mD, or 90.9%, at the end of the loading. At the end of the maximum principal stress σ_1 loading stage, the permeability of the coal samples decreases to 0.0317 mD, a decrease of 0.0503 mD. The permeability of the intermediate stress σ_2 stage is

Equation (16) shows that under the condition of stress path #1, the permeability of the skeletal stratified coal samples is exponentially related to the maximum principal stress, the intermediate principal stress and the minimum principal stress; this finding is in agreement with the vertical bedding theory. The permeability of the stratified coal samples exhibited the same trend. As the stress increased, the permeability of the coal samples with slanted bedding gradually decreased. The fractures in stratified coal samples were gradually compressed and closed in the initial stage of the maximum principal stress loading. The maximum decrease in permeability was 67.4%, which is between the reductions observed for parallel bedding and vertical bedding. Moreover, the decrease in the permeability of the stratified coal samples was 21.3% during the intermediate stress loading stage, and the minimum decrease in permeability was only 11.3%. The result of the rate of decrease to a specific permeability is calculated as follows.

According to Eq. (17), the values of the maximum principal stress σ_1, the intermediate principal stress σ_2 and the minimum principal stress σ_3 are different. During the loading phase, the permeabilities of the coal samples can be expressed as follows.

$$\begin{cases} D_{\text{m1}} = \dfrac{k_0 - k_{\text{m1}}}{k_{\text{b}}} \times 100\% = 67.4\% \\ D_{\text{m2}} = \dfrac{k_0 - k_{\text{m2}}}{k_{\text{b}}} \times 100\% = 21.3\% \\ D_{\text{m3}} = \dfrac{k_0 - k_{\text{m3}}}{k_{\text{b}}} \times 100\% = 11.3\% \end{cases} \tag{17}$$

According to the experimental results of the skeletal coal permeability, the relationship between the effective stress and permeability during the entire loading phase was analyzed, and the variation in the permeability during the entire loading process is fitted as shown in Fig. 16.

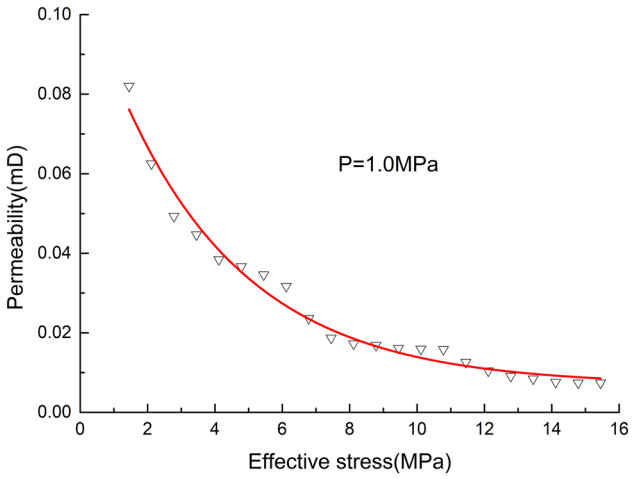

Fig. 16 Relationship between the effective stress and permeability of the coal samples with skewed bedding

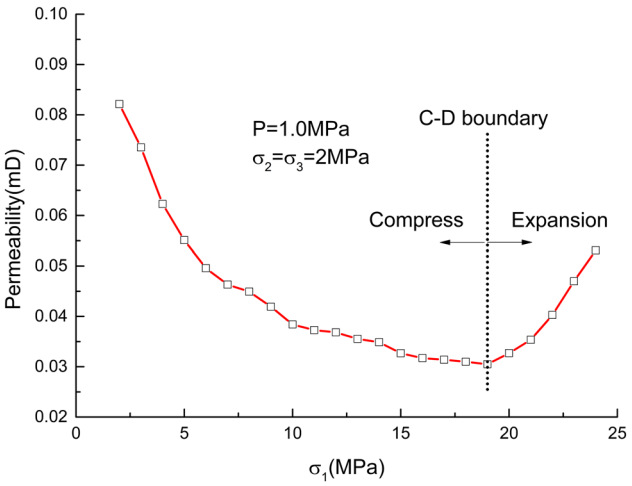

Fig. 17 Effect of the maximum principal stress loading failure process on the C–D boundary and permeability change in the coal samples with skewed bedding

An analysis of Fig. 16 indicates that the permeability of the skeletal stratified coal samples decreases as the effective stress increases during the loading process. This finding is consistent with the trends of permeability observed for vertical stratification and parallel stratification. The initial permeability decrease in sample loading is still the largest, and a linear decrease in permeability is observed at a load of 7 MPa. Then, the permeability slowly decreases at loads above 7 MPa. By fitting and analyzing the permeability trends during the loading process of the stratified coal samples, the fitting equation between the permeability and effective stress can be obtained as follows.

$$k = 0.0039 + 0.0219\exp\left[-0.3152\left(\sigma_1\right)\right]\left(R^2 = 0.9923\right) \tag{18}$$

3.3.2 Compression–Expansion Boundary and Permeability Changes in Coal Samples

According to the preselected experimental method and the set conditions of stress path #2, an investigation of the permeability of coal with skewed bedding was conducted using the experimental platform of the true three-axis fluid–structure interaction servo device. First, the three-axis stresses $\sigma_1 = \sigma_2 = \sigma_3 = 2$ MPa, σ_2 and σ_3 remain unchanged, and σ_1 was loaded at 0.1 MPa/step until the coal sample was destroyed at integer-value loads at the start of the seepage test. The experimental results are shown in Fig. 17.

Then, the constant intermediate principal stress σ_2 and the minimum principal stress σ_3 were 2 MPa, the maximum principal stress σ_1 was loaded until the coal sample was destroyed, and the stress loading ceased when the coal sample permeability began to increase. As illustrated in Fig. 17, the permeability decreases sharply at the initial stage of the maximum principal stress σ_1 loading, and the reduction in permeability decreases more slowly when the load exceeds a certain value. When the skeletal stratified coal sample was loaded at the maximum principal stress $\sigma_1 = 19$ MPa, the permeability of the coal sample began to increase, that is, the maximum principal stress corresponding to the C–D boundary of the oblique coal layer is approximately 19 MPa, which is 6 MPa less than that of the coal samples with vertical bedding.

4 Experimental Results and Analysis

A further analysis of the results of the seepage tests shows that the permeability of coal samples with different bedding structures changes with the stress load and that the change in the load directly affects the permeability of the coal sample. The permeability of different layers of coal samples decreases with an increase in the effective stress, and the permeability considerably changes at the initial effective stress, followed by gradual variations as the effective stress increases. The permeability and effective stress exhibit an exponential relationship for the different layers of coal samples, and the experimental results of the seepage tests of different layered coal samples are consistent with the results of Gash et al. When they applied a load to a coal sample of 6.9 MPa, they found that the permeability was 0.6–1.7 mD parallel to the inside of the layer, but the permeability was only 0.00 7 mD perpendicular to the inside of the layer (Gash et al. 1993).

Figure 18 shows the variations in the permeability of different layered coal samples during stress loading. An analysis of Fig. 18 indicates that different bedding orientations have an important effect on the coal sample permeability.

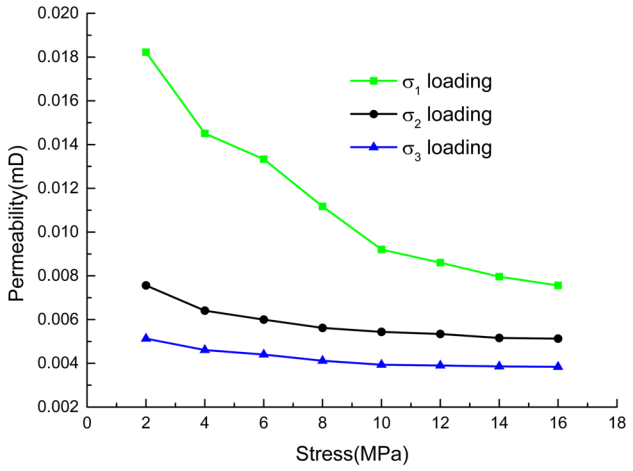

(a) Vertical beddings

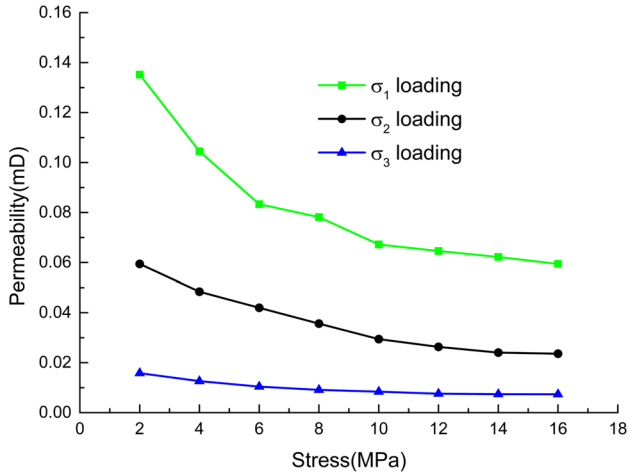

(b) Parallel beddings

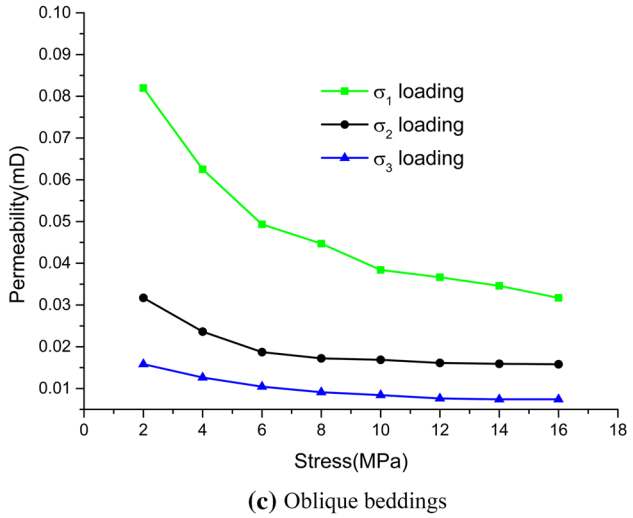

(c) Oblique beddings

Fig. 18 Permeability of the stress loading process for coal samples with different bedding structures: **a** vertical bedding; **b** parallel bedding; and **c** oblique bedding

The initial permeability of the vertically stratified coal samples is 0.0181 mD. The permeability of the coal samples in the final loading stage is reduced to 0.00384 mD, a reduction of 78.9%. The initial permeability of the parallel stratified coal samples is 0.1352 mD, and this value decreases to 0.00635 mD, a decrease of 95.3%, in the late stage of loading. The initial permeability of the vertically stratified coal samples is only parallel to the load direction. The initial permeability of the vertical coal samples was only 13.5% of that of the parallel beddings.

The permeability of the stratified coal samples is 0.0822 mD, and the permeability reaches 0.00739 mD, a decrease of 90.9%, at the end of the loading. The initial permeability of the vertically stratified coal samples is only 22.2% of that for the skewed coal structure. The results show that the direction of bedding has an important influence on the seepage characteristics of the coal samples. In the past, most scholars ignored the influence of bedding when conducting permeability tests.

The permeability of the different stratified coal samples is exponentially related to the maximum principal stress, intermediate principal stress and minimum principal stress. In the initial stage of maximum principal stress loading, the fractures of vertically stratified coal samples are more likely to be compressed and closed. The permeability decreases in this stage, and the maximum decrease is 74.1%. The permeability decreases of coal samples with parallel and skewed strata are 58.8% and 67.4%, respectively. The decreases in the permeability of coal samples with vertical, parallel and skewed stratification in the intermediate stress loading stage are 16.9%, 27.8% and 21.3%, respectively. The minimum permeability decrease in vertically stratified coal samples in the minimum stress period is only 9.0%, and those of coal samples with parallel and skewed structures are 13.4% and 11.3%, respectively. When the maximum principal stress of coal samples with different structures is reached, the initial stage of stress loading is observed, and the pore fissures of the coal samples are rapidly compressed. Therefore, the reduction in the stress load reaches a maximum, and the parallel stratified coal samples exhibit relatively small reductions because the loading direction of the maximum principal stress is parallel to the direction of the stratified fissure plane of the samples. The loading in this stage is unlikely to fully close the stratified fissure plane, and the effects of the intermediate principal stress and minimum principal stress on the permeability of coal are different. The results of this study show that it is unreasonable to simplify the equivalent confining pressure of the intermediate principal stress and the minimum principal stress, as was done in previous seepage tests.

5 Conclusions

1. The initial permeabilities of coal samples with vertical, parallel and skewed stratification were 0.0181, 0.1352 and 0.0822 mD, respectively. The initial permeability of vertically stratified coal samples was only 13.5% and 22.2% of that of coal samples with parallel stratification and skewed stratification, respectively. The permeabilities of coal samples with vertical, parallel and skewed stratification were 0.00384, 0.00635 and 0.00739 mD, respectively, representing permeability decreases of 78.9%, 95.3% and 90.9%. These findings further indicate that the orientation characteristics of the bedding structure have a significant influence on the coal seepage flow.
2. The permeability of different stratified coal samples is exponentially related to the maximum principal stress, intermediate principal stress and minimum principal stress. The general expression is $k = a + b\exp\left[-c\left(\sigma_i\right)\right](i = 1 - 3)$, and the permeability decreases gradually as the stress increases. Specifically, the maximum principal stress, intermediate principal stress and minimum principal stress decrease by 74.1%, 16.9% and 9.0%, respectively, during the loading phase. The permeability of the parallel stratified coal samples decreases in the maximum principal stress, intermediate principal stress and minimum principal stress loading stages. Notably, the permeability decreases by 67.4%, 21.3% and 11.3% in the maximum principal stress, intermediate principal stress and minimum principal stress loading stages, respectively, for coal samples with parallel bedding and by 58.8%, 27.8% and 13.4% for samples with skewed bedding. The loading stage of the maximum principal stress of the coal samples is the initial stage of stress loading. The load in this stage causes the pore fissures of the coal samples to compress rapidly, which results in the maximum decrease in permeability, which varies based on differences in the bedding structure direction. There is a large difference between the magnitudes of the permeability variations.
3. The permeability of the different stratified coal samples decreases as the effective stress increases, and the permeability and effective stress exhibit an exponential relationship. The general expression is $k = a + b\exp\left[-c\left(\sigma_e\right)\right]$, and the decrease in the initial permeability in vertically stratified coal samples is relatively large. The permeability decreases linearly when the effective stress is loaded to 8 MPa, and it decreases slowly when the load exceeds 8 MPa. The permeability of parallel layered coal samples decreases linearly when the effective stress is loaded to 10 MPa; above 10 MPa, the decrease in permeability gradually diminishes. The permeability decreases linearly when the effective stress is loaded to 7 MPa and then decreases gradually above 7 MPa. Then, an increase in the effective stress leads to a decrease in the permeability of the coal samples. However, the change in the coal sample permeability gradually stabilizes after a certain value is reached. The deformation and failure processes of coal samples with different bedding strata sharply decrease in the initial stage of stress loading, and the rate of decrease in the permeability decelerates as the stress increases. When the coal samples with vertical, parallel and skewed strata are loaded to 25, 22 and 19 MPa, respectively, the permeability begins to increase, and the coal samples gradually enter the stage of expansion and deformation. Thus, the maximum principal stresses corresponding to the C–D boundaries of vertical, parallel and oblique cross-stratified coal samples are 25, 22 and 19 MPa, respectively.
4. With the intermediate principal stress σ_2 and minimum principal stress σ_3 held constant ($\sigma_2 = \sigma_3 = 2$ MPa), the maximum principal stress σ_1 is loaded until the coal sample is destroyed, and the loading of the maximum principal stress σ_1 ceases when the permeability increases. The deformation and failure processes of coal samples with different bedding strata sharply decrease at in the initial stage of stress loading, and the permeability decreases slowly as the stress increases. When the coal samples with vertical, parallel and skewed strata are loaded to 25, 22, and 19 MPa, respectively, the permeability begins to increase, and the coal samples gradually enter the stage of expansion and deformation. Thus, the maximum principal stresses corresponding to the C–D boundaries of vertical, parallel and obliquely bedded coal samples are 25, 22 and 19 MPa, respectively.

Acknowledgements This work was supported by National Natural Science Foundation of China (51604101, 51704099, 51734007, 51774119, and 51604092), the National Key Research and Development Program of China (2018YFC0808103), the Doctoral Fund of Henan Polytechnic University (no. B2018-59), the State Key Laboratory Cultivation Base for Gas Geology and Gas Control (Henan Polytechnic University) (WS2017B06), the Henan Postdoctoral Foundation, and the Open Research Fund Program of Hunan Province Key Laboratory of Safe Mining Techniques Of Coal Mines (Hunan University of Science and Technology) (201502), the Open Research Fund Program of Hunan Province Key Laboratory of Safe Mining Techniques Of Coal Mines (Hunan University of Science and Technology) (201502).

References

Cristescu N et al (1994) A procedure to determine non-associated constitutive equations for geomaterials. Int J Plast 10(2):103–131

Deng GH, Shao SJ (2013) Research on change structural characteristics of loess based on true triaxial tests. Rock Soil Mech 03:679–684

Du K, Li XB, Li DY, Weng L (2013) Failure properties of rocks in true triaxial unloading compressive test. Trans Nonferrous Metals Soc China 25:571–581

Faoro I, Niemaijer A, Marone C (2009) Influence of shear and deviatoric stress on the evolution of permeability in fractured rock. J Geophys Res Solid Earth 114:B1

Feng XT, Zhang XW, Kong R (2016) A novel mogi type true triaxial testing apparatus and its use to obtain complete stress-strain curves of hard rocks. Rock Mech Rock Eng 49:1649–1662

Gao YB, Liu DQ, Zhang XY (2017) Analysis and optimization of entry stability in underground longwall mining. Sustainability 9(11):2079

Gash BW, Volz RF, Potter G (1993) The effects of cleat orientation and confining pressure on cleat porosity, permeability and relative permeability in coal. Paper 93(21):17–21

Gong WL, Feng XW, Hu AQ, Du S, Zhao ZH (2011) Experimental study on real triaxial physical simulation of coal seam gas seepage. Beijing Mech Assoc 08:330–338

Huang BX, Li PF (2015) Experimental investigation on the basic law of the fracture spatial morphology for water pressure blasting in a drillhole under true triaxial stress. Rock Mech Rock Eng 48:1699–1709

Ingraham MD, Issen KA, Holcomb DJ (2013) Response of castlegate sandstone to true triaxial states of stress. J Geophys Res Solid Earth 118:536–552

Kaunda R (2014) New artificial neural networks for true triaxial stress state analysis and demonstration of intermediate principal stress effects on intact rock strength. J Rock Mech Geotech Eng 6:338–347

Karev VI, Klimov DM, Kovalenko YuF (2016) Fracture of sedimentary rocks under a complex triaxial stress state. Mech Solids 51(5):522–526

Klimov DM, Kovalenko YF (2016) Fracture of sedimentary rocks under a complex triaxial stress state. Mech Solids 51:522–526

Kwasniewski M (2013) Recent advances in studies of the strength of rocks under true triaxial compression conditions. Arch Min Sci 58:1177–1200

Lei QH, Wang XG, Xiang JS (2017) Polyaxial stress-dependent permeability of a three-dimensional fractured rock layer. Hydrogeol J 25:2251–2262

Li DQ, Zhang SC, Zhang SA (2014) Experimental and numerical simulation study on fracturing through interlayer to coal seam. J Nat Gas Sci Eng 21:386–389

Li MH, Yin GZ, Xu J (2016a) Permeability evolution of shale under anisotropic true triaxial stress conditions. Int J Coal Geol 08:142–148

Li WX, Wang G, Du WZ (2016b) Development and application of a true triaxial gas-solid coupling testing system for coal seepage. Rock Soil Mech 37:2109–2118

Li MH, Yin GZ, Xu J (2016c) A novel true triaxial apparatus to study the geomechanical and fluid flow aspects of energy exploitations in geological formations. Rock Mech Rock Eng 49:4647–4659

Liu YB, Li MH, Yin GZ, Zhang DM, Deng BZ (2018) Permeability evolution of anthracite coal considering true triaxial stress conditions and structural anisotropy. J Nat Gas Sci Eng 52:492–506

Massarotto P, Rudolph V, Golding SD (2003) Anisotropic permeability characterisation of permian coals. In: International coalbed methane symposium. The University of Alabama, pp 1–11

Miao JL, Jia XN, Cheng C (2011) The failure characteristics of granite under true triaxial unloading condition. Procedia Eng 26:1620–1625

Mosleh MH, Turner M, Sedighi M, Vardon PJ (2018) Carbon dioxide flow and interactions in a high rank coal: permeability evolution and reversibility of reactive processes. Int J Greenhouse Gas Control 70:57–67

Nasseri MHB, Goodfellow SD, Lombos L (2014) 3-D transport and acoustic properties of fontainebleau sandstone during true-triaxial deformation experiments. Int J Rock Mech Min Sci 69:1–18

Nie MS, He XQ, Li XC, Zhang X (2009) Experimental study on gas seepage law of coal under true triaxial stress. Chin Soc Rock Mech Eng 26:354–356

Niu Y, Mostaghimi P, Shikhov I, Chen Z, Armstrong RT (2018) Coal permeability: gas slippage linked to permeability rebound. Fuel 215:844–852

Samuelson J, Elsworth D, Marone C (2009) Shear-induced dilatancy of fluid-saturated faults: experiment and theory. J Geophys Res Solid Earth 114:B12

Shi R, Liu J, Wei M, Elsworth D, Wang X (2018) Mechanistic analysis of coal permeability evolution data under stress-controlled conditions. Int J Rock Mech Min Sci 110:36–47

Takahashi M (2007) Permeability and deformation characteristics of shirahama sandstone under a general stress state. Arch Min Sci 52:355–369

Takahashi M, Park H, Takahashi N (2013) True triaxial tests-using permeability and extensional stress parameters to simulate geological history in rocks. Geosyst Eng 16:75–82

Tan P, Jin Y, Han K (2017) Vertical propagation behavior of hydraulic fractures in coal measure strata based on truetriaxial experiment. J Petrol Sci Eng 158:398–407

Wang K, Zhang J (2013) Comparison between cleat aperture-dependent and porosity-dependent permeability models for triaxial stress conditions. Disaster Adv 6:185–192

Wang DK, Wei JP, Yin GZ (2012) Investigation on change rule of permeability of coal containing gas under complex stress paths. Chin J Rock Mech Eng 2:303–310

Wang DK, Wei JP, Fu QC (2015) Seepage law and permeability calculation of coal gas based on Klinkenberg effect. J Cent South Univ 22:1973–1978

Xie HQ, He CH (2010) Study of the unloading characteristics of a rock mass using the triaxial test and damage mechanic. Int J Rock Mech Min Sci 47(2):286–298

Xu ZW (2003) Study on the characteristic of soil anisotropic deformation by true triaxial test. HeHai University, Nanjing

Xu J, Peng S, Yin GZ, Tao YQ, Yang HW, Wang WZ (2010) Development and application of triaxial servo-controlled seepage equipment for thermofluid-solid coupling of coal containing methane. Chin J Rock Mech Eng 05:2436–2445

Yin GZ, Li MH, Xu J, Wang WZ, Li WP, Li X, Song ZL, Deng BZ (2015) A new multifunctional true triaxial fluid-solid coupling experiment system and its applications. Chin J Rock Mech Eng 12:2436–2445

Zhang KY, Zhu JG, Wu XM (2010) True triaxial test on clay mixed with gravel under complex stress state. Rock Soil Mech 31:2799–2804

Zhao XG, Cai M (2015) Influence of specimen height-to-width ratio on the strainburst characteristics of Tianhu granite under true-triaxial unloading conditions. Can Geotech J 52:890–902